

Stepping Stone Mechanism: Carrier-Free Long-Range Magnetism Mediated by Magnetized Cation States in Quintuple Layer *

Chunkai Chan(陈俊佳), Xiaodong Zhang(张小东), Yiou Zhang(张异欧), Kin-fai Tse(谢建辉), Bei Deng(邓贝), Jingzhao Zhang(张璟昭), Junyi Zhu(朱骏宜)

¹Department of Physics, Chinese University of Hong Kong, Hong Kong

(Received 19 October 2017)

The long-range magnetism observed in group-V tellurides quintuple layers is the only working example of carrier-free dilute magnetic semiconductors (DMS), whereas the physical mechanism is unclear, except the speculation on the band topology enhanced van Vleck paramagnetism. Based on DFT calculations, we find a stable long-range ferromagnetic order in a single quintuple layer of Cr-doped Bi_2Te_3 or Sb_2Te_3 , with the dopant separation more than 9 \AA . This configuration is the global energy minimum among all configurations. Different from the conventional super exchange theory, the magnetism is facilitated by the lone pair derived anti-bonding states near the cations. Such anti-bonding states work as stepping stones merged in the electron sea and conduct magnetism. Further, spin orbit coupling induced band inversion is found to be insignificant in the magnetism. Therefore, our findings directly dismiss the common misbelief that band topology is the only factor that enhances the magnetism. We further demonstrate that removal of the lone pair derived states destroys the long-range magnetism. This novel mechanism sheds light on the fundamental understanding of long-range magnetism and may lead to discoveries of new classes of DMS.

PACS: 75.50.Pp, 71.15.Mb, 71.70.Gm, 75.30.Hx

DOI: 10.1088/0256-307X/35/1/017502

The stable magnetism in 2D materials has been challenging and critical to realize new spintronic devices for decades. Recently, there are some developments in the realization of 2D magnetic transition metal compound.^[1–3] Nevertheless, the carrier-independent ferromagnetism and anti-ferromagnetism in 2D or thin film dilute magnetic semiconductors remain to be extremely difficult to realize.^[4] In such applications, an ideal purpose of free carrier manipulation is to realize the desired electronic functions with magnetic properties unchanged. However, in reality, it is almost unavoidable to tune both properties simultaneously. Very recently, it has been demonstrated that a long-range ferromagnetism, independent of both polarity and density of free carriers or even without carriers, can exist in Cr- or V-doped $(\text{Bi}_x\text{Sb}_{1-x})_2\text{Te}_3$ thin film or multiple quintuple layers, leading to the discovery of the quantum anomalous Hall effect.^[5–13] One of keys to the success is the long-range ferromagnetism, while the underlying physical mechanism is still largely unclear.

$(\text{Bi}_x\text{Sb}_{1-x})_2\text{Te}_3$ is a typical topological insulator with conducting surface states and insulating bulk states, protected by time reversal symmetry.^[14] The introduction of magnetic dopants, such as Cr, may break the time reversal symmetry and affect the topological surface states.^[15–19]

In this DMS quasi 2D system, the long-range magnetic interaction network contains both cation sites and anion sites of host materials that connect mag-

netic dopants. The usual super exchange theory that focuses on response of mediated anions cannot explain the long-range ferromagnetism in this system.^[20–22] As we shall show, the states near cations in the network may make significant contribution to the long-range magnetic interactions. On the other hand, the present theory proposed to explain the long-range ferromagnetism mechanism emphasizes on the topological non-trivial band structure.^[15] In this attempt, however, only the enhanced paramagnetic susceptibility in undoped topological insulators was estimated, and no mutual interaction between magnetic dopants with large separations was calculated. In addition, no theoretical analysis was performed to study the difference between similar material family of Bi_2Te_3 , Sb_2Te_3 and Bi_2Se_3 . Later numerical works based on small supercells can hardly convince the existence of the long-range magnetism.^[23,24] Also, one work estimated long-range magnetic coupling constants in the presence of carriers in a few configurations without analyzing the stability of the dopants.^[25] Therefore, the systematic analysis of carrier free magnetism in such systems is missing. Also, in most of the previous works, the dopant concentration is higher than experimental value and may lead to some unphysical results.^[23,24] However, in our calculations, the simulation cell is intentionally chosen to have the similar dopant concentration as experimental ones. In addition, the carrier free nature of our calculation guarantees the correct occupations of electrons and avoids

*Supported by Chinese University of Hong Kong (CUHK) under Grant No 4053084, University Grants Committee of Hong Kong under Grant No 24300814, and the Start-up Funding of CUHK.

**Corresponding author. Email: jy Zhu@phy.cuhk.edu.hk

© 2018 Chinese Physical Society and IOP Publishing Ltd

the common mistakes in early literature on DMS.^[26,27]

In this Letter, we investigate the mechanism for the long-range ferromagnetism in Cr-doped topological insulators by performing *ab initio* calculations within the density functional theory (DFT) framework implemented in VASP code with a sufficiently large simulation cell^[28] (refer to SI-A for computational details). To avoid further complexity of alloy effects in $(\text{Bi}_x\text{Sb}_{1-x})_2\text{Te}_3$, we calculate the magnetic order of Cr doped Bi_2Te_3 , Sb_2Te_3 and Bi_2Se_3 , respectively. To our surprise, we discover a novel long-range ferromagnetic (FM) order in carrier free Bi_2Te_3 and Sb_2Te_3 single quintuple layer. In addition, these configurations are the most stable for a single quintuple layer only. This finding is independent of the band topology. The similar ferromagnetic order is relatively unstable for Bi_2Se_3 , consistent with the experimental results.^[29] Later, we use Bi_2Te_3 as a model system to illustrate the origin of the magnetism and qualitatively explain the intriguing interaction based on an extended Hubbard model.^[30]

To study the long-range magnetic order of the Cr-doped Bi_2Se_3 , Bi_2Te_3 , and Sb_2Te_3 thin films, we first replace two Bi or Sb atoms with two Cr atoms in the 4×4 host cell that contains one quintuple layer (details can be found in Fig. S1 of the Supplemental Material).

The relative formation energy is defined as the energy difference between the formation energy of a configuration and that of the most stable configuration, as shown in Fig. 1(a). Significant formation energy drops on the seventh neighboring sites are found in all the systems. These configurations are the global minima in Bi_2Te_3 and in Sb_2Te_3 , which are even more stable than the first or second nearest neighbor ones. On the other hand, the second nearest neighbor configuration is the most stable in Bi_2Se_3 . As a function of the distance between the neighboring Cr atoms, the relative formation energy of Cr dopants in these three materials shows generally similar trends.

Since the global minimum of the formation energy of Cr atoms in the Bi_2Se_3 thin film is the second nearest neighbor configuration, Cr atoms tend to form clusters in Bi_2Se_3 , leading to nonmagnetic or paramagnetic orders. On the contrary, the global minimum of the formation energies of Cr atoms in the telluride suggests a long-range ferromagnetism order. These results qualitatively agree with the experimental observations.^[5,29]

We also calculate the ferromagnetic coupling constants vs the neighboring sites, as shown in Fig. 1(b). The coupling constants are defined as half of the energy difference between the two Cr atoms with the same spins (ferromagnetism) and the two atoms with opposite spins (anti-ferromagnetism). We find that the seventh nearest neighbor configurations favor ferromagnetism and yield coupling constants about 6 meV for all systems, despite the fact that the cou-

pling strength is lower than the first or second nearest neighbor configurations. Also, the periodic images of the dopants may enhance the magnetism. This is physical because our simulated concentration is close to the experimental values. Also, calculations based on large cells without the enhancement of the periodic images demonstrate ferromagnetism (see SI-B and Fig. S2 for details).

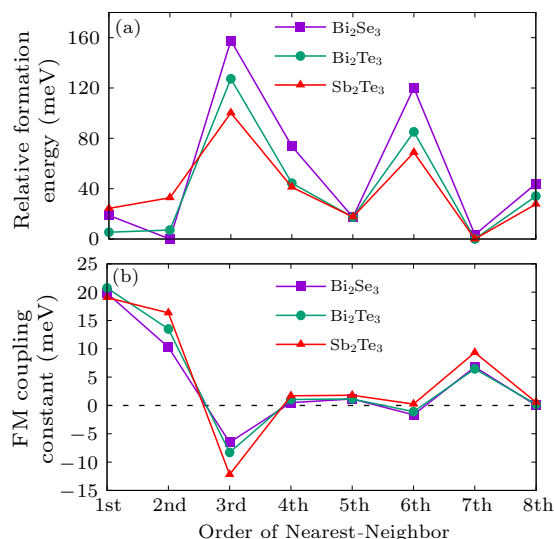


Fig. 1. (a) The relative formation energy of two-Cr-atom doped (4×4 supercell) single quintuple layer of Bi_2Se_3 (purple square), that of Bi_2Te_3 (green circle), and that of Sb_2Te_3 (red triangle) with respect to different neighboring sites of the Cr atoms. (b) The ferromagnetic coupling constants of the same systems

These findings are novel because the coupling strength in common DMS decays very fast in respect to the separation distances.^[31] However, in our seventh nearest neighbor configuration, the two Cr atoms are separated by two anion atoms and one Bi atom. Also note that the difference between the formation energy on the seventh nearest neighboring sites and that on the first (or second) nearest neighboring sites in Sb_2Te_3 is the largest among these three systems. These results match with the experimental findings that quantum anomalous Hall effect can be realized in the Sb rich $(\text{Bi}_x\text{Sb}_{1-x})_2\text{Te}_3$.^[5]

In order to check the accuracy of GGA results in the slab model, we also calculate the formation energy and the coupling constants using the GGA+U method with spin orbit coupling (SOC) included. We find that GGA+U and SOC do not change the conclusions of the GGA results (more details are shown in Fig. S3). Furthermore, calculations about Cr doped bulk Bi_2Te_3 also show the similar trend (refer to Fig. S4 and Fig. S5).

Based on the above discussions, both GGA and GGA+U plus SOC yield similar results. Therefore, we only include the GGA results on slab models in the following discussions.

To understand the origin of such long-range ferro-

magnetism, we further study the intrinsic electronic properties of Bi_2Te_3 . The projected density of states (pDOS) of Bi $6s$ and Te $5p$ are shown in Fig. 2(a). Despite the local symmetry difference, two Te atoms at different sites yield similar $5p$ orbital components, so we choose one Te atom to show these orbitals. From the pDOS figure, it is clear that the dominant component of the valence band is Te $5p$. Additionally, the majority of the Bi $6s$ state, as a nonbonding lone pair state, is deep under the valence band maximum (VBM). However, a relatively small portion of Bi $6s$ state is found to be slightly below the VBM. These results suggest that the small portion couples with the Te $5p$ orbital and forms an occupied sp anti-bonding (anti- $sp\sigma$) state.

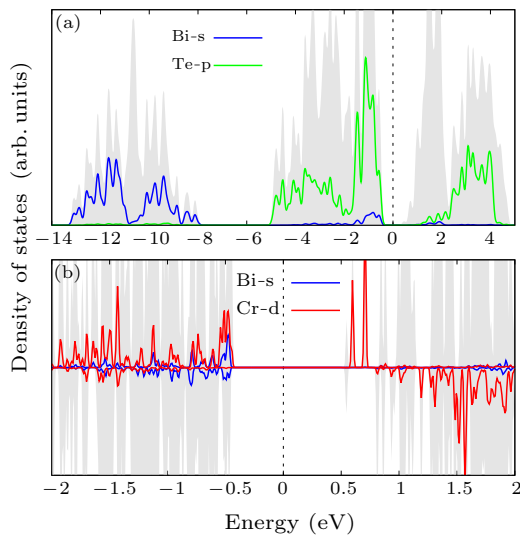


Fig. 2. (a) The pDOS of the Bi $6s$ orbital (blue) and Te $5p$ orbital (green) in pure Bi_2Te_3 . The total density of states is shown in the grey shading background. The dotted line shows the Fermi level. (b) The pDOS of the Cr $3d$ orbital (red) and the $6s$ orbital of the Bi (blue) (Bi atom on the Cr-Te-Bi-Te-Cr path) in single Cr-doped Bi_2Te_3 . The grey background is the total DOS of single Cr-doped Bi_2Te_3 , and the positive and negative values represent the pDOS of spin-up and spin-down components, respectively.

Next, we study the single Cr-doped Bi_2Te_3 . Cr dopant has 3 unpaired $3d$ electrons with a magnetic moment of $3\mu_B$. The pDOS of the Cr $3d$ orbitals and the $6s$ orbital of the Bi next to the Cr dopant are calculated, as shown in Fig. 2(b). The significant asymmetric nature of the spin-up and spin-down portion of the Bi $6s$ orbital suggests that it is magnetized by the nearby Cr atom. Therefore, the anti- $sp\sigma$ state is also magnetized. It should be noted that the anti- $sp\sigma$ state is an intrinsic property of Bi_2Te_3 . We calculate the partial charge density of the second band below VBM (Fig. S6). The charge density in vicinity to the Bi atom shows the shape of the anti- $sp\sigma$ state. The role of Cr dopant is to magnetize it, but not to create it. The pDOS of Cr $3d$ also indicates that there is a small occupation of spin-down component, leading to the magnetization of the surrounding atoms.

To understand the magnetization of surrounding atoms, we further calculate the spin density of single Cr-doped Bi_2Te_3 , as shown in Fig. 3(a), where only the spin polarized atoms are displayed. We find that the neighboring p orbitals of Te are magnetized along the bonding direction between Te and Cr atoms, which we label as p_z orbital (note that z axis is along the local bonding direction). The total magnetization of all the Te p orbitals is anti-parallel to the Cr magnetic moment. These results are in good agreement with the experimental observations.^[32] The spin density also suggests that the spin up electron cloud near the Bi atom is the anti- $sp\sigma$ state, which also couples to the Cr atom. Interestingly, the Cr-Te-Bi chain forms a right angle, as shown in Fig. 3(b). Note that such chains are fundamental building blocks to form the long-range magnetic order, as further studies suggest.

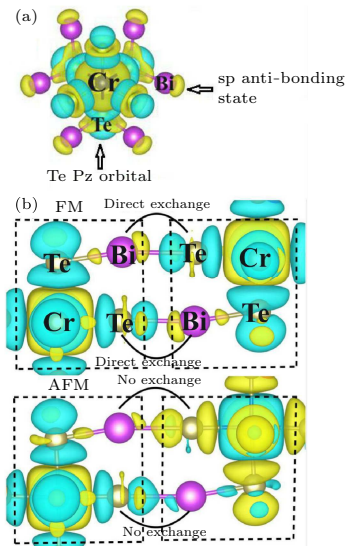


Fig. 3. Spin density of single and two Cr doped Bi_2Te_3 . Large purple atom is Bi, cinnamon atom is Te, blue atom (central atom) is Cr. (a) The spin density of the single Cr-doped Bi_2Te_3 with Cr in the center. Center Cr atom is surrounded by six Te atoms. Bi atoms bonding to Te atoms. (b) The spin density of two adjacent magnetic blocks in ferromagnetism and anti-ferromagnetism states. The spin-up and spin-down density are yellow and blue, respectively, in both figures.

The spin polarized results can be qualitatively understood based on an electron hopping mechanism. Since the electronic environment around the Cr atom is approximately O_h symmetry, the Cr $3d$ orbitals are split into filled spin-up t_{2g} states and empty e_g states. Due to the local symmetry, the Te p_z orbital is only coupled to the Cr e_g states. Since the energy of the spin-up e_g states is lower than that of the spin-down component, a portion of spin-up electrons of the Te p_z orbital hops to the e_g state. As a result, the p_z orbital is magnetized towards spin down. Since the t_{2g} states are already occupied by three spin up electrons, only spin-down electrons in the anti- $sp\sigma$ state can hop to the t_{2g} states. As a result, the anti- $sp\sigma$

state is magnetized towards spin up.

These results also indicate that the magnetic moments of the Cr atom are not fully localized at the Cr site and a small portion of them are distributed in the surrounding orbitals. Still, the magnetic moment in the Te p states cannot be interpreted as spin polarized hole states,^[32] because the Cr-doped Bi_2Te_3 thin films remain carrier-free.

As shown in Fig. 3(b), when two of these building blocks are placed in adjacent to each other, long-range ferromagnetic interaction can occur, with the two Cr atoms at seventh nearest neighboring sites. In the ferromagnetic configuration, the spin of the anti- $sp\sigma$ orbitals in one block and the adjacent p_z orbitals in the other block are anti-parallel. Therefore, electron hopping between these orbitals lowers their kinetic energy. However, in the anti-ferromagnetic configuration, these two spins are parallel and electron hopping cannot lower the energy. As a result, the ferromagnetic configuration is energetically favorable. Such building blocks further connect and form a strong ferromagnetic network in the whole crystal. In this novel scheme, the anti-bonding state near the middle cation serves as an essential stepping stone to mediate the magnetic interaction. Therefore, we name this mechanism as a stepping stone mechanism and these Bi atoms connecting the two building blocks are at stepping stone sites. Also, this effect is different from the traditional super exchange theory, which provides no discussions on the role of intermediate cation states.^[20–22]

To validate our new mechanism, we replace Bi atoms at the stepping stone sites with Ga atoms that do not have lone pair electrons, but share the same valence as Bi atoms. Due to the periodic boundary condition, the two adjacent building blocks in $4 \times 4 \text{ Bi}_2\text{Te}_3$ supercell have four stepping stone sites. We replace Bi atoms at the sites one by one by Ga atoms and calculate the magnetic coupling strength, as shown in Fig. 4(a). The magnetic coupling constant decreases approximately linearly with the number of the replacements and finally vanishes when all four Bi atoms are replaced. In contrary to the Ga replaced case, the magnetic interaction remains approximately unchanged when Sb atoms substitute the stepping stone Bi atoms. These results are also qualitatively consistent with the ferromagnetism order observed in $(\text{Bi}_x\text{Sb}_{1-x})_2\text{Te}_3$.^[5] To further demonstrate the unique properties of the Bi atoms at the stepping stone sites, we also replace the Bi atoms that are not at the stepping stone sites, but still in the same quintuple layer, by Ga atoms and find that the ferromagnetic order preserves since the coupling constants almost do not change even when four non-stepping-stone Bi atoms are replaced. These results confirm our mechanism.

Finally, to visualize the disappearance of the anti- $sp\sigma$ state when Bi at the stepping stone site is re-

placed, we calculate the spin density of two touching magnetic blocks with one Bi atom replaced by a Ga atom, as shown in Fig. 4(b) and Fig. 4(c). It clearly shows that the Ga atom does not have a spin polarized anti- $sp\sigma$ orbital, which still can be seen around the remaining Bi atom, as indicated by the arrow in Fig. 4(c). These results also suggest that the missing of such states can be the fundament reason to hinder the long-range magnetism in carrier-free DMS. Also note that, such a mechanism is a necessary condition for long-range magnetism and the formation energy of this configuration is required to be the global minimum to achieve DMS.

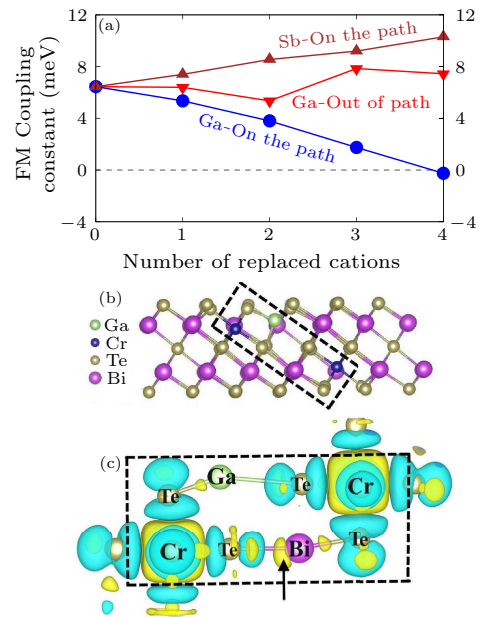


Fig. 4. (a) The ferromagnetic coupling constant with respect to the number of Ga and Sb atoms replacing the Bi atoms at the stepping stone sites (blue and brown, respectively), or at the non-stepping stone sites (red). (b) The $4 \times 4 \text{ Bi}_2\text{Te}_3$ simulation cell with the seventh neighboring sites doped with Cr atoms and one Bi atom at the stepping stone site replaced by a Ga atom (green). (c) The spin density of two adjacent magnetic blocks with one Ga atom replacing one Bi atom at the stepping stone site. The yellow and blue colors represent the spin-up and spin-down densities, respectively. The sp anti-bonding state is marked by the arrow

Our new discovery suggests that during the crystal growth stage, there exists a thermodynamic driving force that separates the magnetic dopants and forms long-range magnetic order. Of course, after the growth and during the transport measurement, other possible mechanisms, such as surface topological states, can also enhance the magnetism. Still, there are plenty of discussions^[16,19] in this area and it is beyond the scope of this paper.

In summary, we have found a stable carrier independent long-range ferromagnetic interaction in Bi_2Te_3 and Sb_2Te_3 , which agrees well with the experimental results.^[5,6,33,34] An electron hopping mechanism based on the intrinsic anti- $sp\sigma$ state is proposed

to qualitatively explain this intriguing finding. Our further studies also suggest that this mechanism exists in other material systems (not published results). This discovery may greatly enhance the understanding of the hidden and carrier free long-range magnetism, lead to the discoveries of new classes of DMS materials, and widen the material choices of spintronic devices.

References

- [1] Wang X, Du K, Liu Y Y F, Hu P, Zhang J, Zhang Q, Owen M H S, Lu X, Gan C K, Sengupta P, Kloc C and Xiong Q 2016 *2D Mater.* **3** 031009
- [2] Gong C, Li L, Li Z, Ji H, Stern A, Xia Y, Cao T, Bao, W, Wang C, Wang Y, Qiu Z Q, Cava R J, Louie S G, Xia J and Zhang X 2017 *Nature* **546** 265
- [3] Huang B, Clark G, Navarro-Moratalla E, Klein D R, Cheng R, Seyler K L, Zhong D, Schmidgall E, McGuire M A, Cobden D H, Yao W, Xiao D, Jarillo-Herrero P and Xu X 2017 *Nature* **546** 270
- [4] Zhang J, Chang C Z, Zhang Z, Wen J, Feng X, Li K, Liu M, He K, Wang L, Chen X, Xue Q K, Ma X and Wang Y 2011 *Nat. Commun.* **2** 574
- [5] Chang C Z, Zhang J, Feng X, Shen J, Zhang Z, Guo M, Li K, Ou Y, Wei P, Wang L L, Ji Z Q, Feng Y, Ji S H, Chen X, Jia J F, Dai X, Fang Z, Zhang S C, He K, Wang Y Y, Lu L, M X C and Xue Q K 2013 *Science* **340** 167
- [6] Chang C, Zhang J, Liu M, Zhang Z, Feng X, Li K, Wang L, Chen X, Dai X and Fang Z 2013 *Adv. Mater.* **25** 1065
- [7] Chang C Z, Zhao W W, Kim D Y, Zhang H J, Assaf B A, Heiman D, Zhang S C, Liu C X, Chan M H W and Moodera S J 2015 *Nat. Mater.* **14** 473
- [8] Bestwick A J, Fox E J, Kou X, Pan L, Wang, K L and Goldhaber-Gordon D 2015 *Phys. Rev. Lett.* **114** 187201
- [9] Feng Y, Feng X, Ou Y B, Wang J, Liu C, Zhang L G, Zhao D Y, Jiang G Y, Zhang S C, He K, Ma X, Xue Q K and Wang Y 2015 *Phys. Rev. Lett.* **115** 126801
- [10] Feng X, Feng Y, Wang J, Ou Y B, Hao Z Q, Liu C, Zhang, Z C, Zhang L G, Lin C X, Liao J, Li Y Q, Wang L L, Ji S H, Chen X, Ma X C, Zhang S C, Wang Y Y, He K and Xue Q K 2016 *Adv. Mater.* **28** 6386
- [11] Kou X F, Guo S T, Fan Y B, Pan L, Lang M R, Jiang Y, Shao Q M, Nie T X, Murata K, Tang J S, Wang Y, He L, Lee T K, Lee W L and Wang K L 2014 *Phys. Rev. Lett.* **113** 137201
- [12] Kou X, Fan Y, Lang M, Upadhyaya P and Wang K L 2015 *Solid State Commun.* **215-216** 34
- [13] Kou X F, Pan L, Wang J, Fan Y B, Choi E S, Lee W L, Nie T X, Murata K, Shao Q M, Zhang S C and Wang K L 2015 *Nat. Commun.* **6** 8474
- [14] Zhang H J, Liu C X, Qi X L, Dai X, Fang Z and Zhang S C 2009 *Nat. Phys.* **5** 438
- [15] Yu R, Zhang W, Zhang H J, Zhang S C, Dai X and Fang Z 2010 *Science* **329** 61
- [16] Chen Y L, Chu J H, Analytis J G, Liu Z K, Igarashi K, Kuo H H, Qi X L, Mo S K, Moore R G, Lu D H, Hashimoto M, Sasagawa T, Zhang S C, Fisher I R, Hussain Z and Shen Z X 2010 *Science* **329** 659
- [17] Hasan M Z and Kane C L 2010 *Rev. Mod. Phys.* **82** 3045
- [18] Qi X and Zhang S 2011 *Rev. Mod. Phys.* **83** 1057
- [19] Checkelsky J G, Ye J, Onose Y, Iwasa Y and Tokura Y 2012 *Nat. Phys.* **8** 729
- [20] Anderson P W 1950 *Phys. Rev.* **79** 350
- [21] Goodenough J B 1955 *Phys. Rev.* **100** 564
- [22] Kanamori J 1959 *J. Phys. Chem. Solids* **10** 87
- [23] Zhang J M, Zhu W G, Zhang Y, Xiao D and Yao Y G 2012 *Phys. Rev. Lett.* **109** 266405
- [24] Deng B, Zhang Y O, Zhang S B, Wang Y Y, He K and Zhu J Y 2016 *Phys. Rev. B* **94** 054113
- [25] Vergniory M G, Otrokov M M, Thonig D, Hoffmann M, Maznichenko I V, Geilhufe M, Zubizarreta X, Ostanin S, Marmodoro A, Henk J, Hergert W, Mertig I, Chulkov E V and Ernst A 2014 *Phys. Rev. B* **89** 165202
- [26] Sato K, Bergqvist L, Kudrnovský J, Dederichs P H, Eriksson O, Turek I, Sanyal B, Bouzerar G, Katayama-Yoshida H, Dinh V A, Fukushima T, Kizaki H and Zeller R 2010 *Rev. Mod. Phys.* **82** 1633
- [27] Zunger A, Lany S and Raebiger H 2010 *Physics* **3** 53
- [28] Kresse G and Furthmüller J 1996 *Phys. Rev. B* **54** 11169
- [29] Chang C Z, Tang P, Wang Y L, Feng X, Li K, Zhang Z, Wang Y, Wang L L, Chen X, Liu C, Duan W, He K, Ma X C and Xue Q K 2014 *Phys. Rev. Lett.* **112** 056801
- [30] Slipukhina I, Mavropoulos P, Blügel S and Ležaić M 2011 *Phys. Rev. Lett.* **107** 137203
- [31] Plötz W, Fabian J and Hohenester U 2007 *Modern Aspects of Spin Physics* (Berlin: Spinger)
- [32] Ye M, Li W, Zhu S, Takeda Y, Saitoh Y, Wang J, Pan H, Nurmatamat M, Sumida K and Ji F 2015 *Nat. Commun.* **6** 8913
- [33] Dyck J S, Drašar Ć, Lošt'ák P and Uher C 2005 *Phys. Rev. B* **71** 115214
- [34] Zhou Z, Chien Y J and Uher C 2006 *Phys. Rev. B* **74** 224418

Supplementary Material: Stepping Stone Mechanism: Carrier-Free Long-Range Magnetism Mediated by Magnetized Cation States in Quintuple Layer*

Chunkai Chan(陈俊佳), Xiaodong Zhang(张小东), Yiou Zhang(张异欧), Kinlai Tse(谢建辉), Bei
Deng(邓贝), Jingzhao Zhang(张璟昭), and Junyi Zhu(朱骏宜)**

Department of Physics, Chinese University of Hong Kong, Hong Kong SAR, China

*Supported by Chinese University of Hong Kong (CUHK) (Grant No.4053084), University Grants
Committee of Hong Kong (Grant No. 24300814), and start-up funding of CUHK.

**Email: jyzhu@phy.cuhk.edu.hk

Text A: Computational Methods and Details

All calculations are performed using projected augmented wave (PAW) [1] potentials with Perdew-Burke-Ernzerhof (PBE) [2] generalized gradient approximation (GGA) as implemented in Vienna *ab initio* simulation package (VASP) [3]. The cutoff energy for plane-wave expansion was set to 350eV for both Bi₂Se₃ and Bi₂Te₃ and 400eV for Sb₂Te₃. Gamma centered 3×3×1 *k* mesh is used to sample the Brillouin zone for 4×4 supercell of Bi₂X₃ (X=Se, Te) and Sb₂Te₃, as shown in Fig. S1, with all the neighboring sites marked. The number 0 represents the position of first Cr atom. The numbers 1 to 8 represent the 1st to 8th nearest neighbor placements of the second Cr atom. All atoms in every supercell are fully relaxed until the residual force is less than 0.01 eV/Å. Convergence tests about kpoints, cell sizes, vacuum size, magnetism, and energy cutoffs have been performed. The formation energy of the dopants is defined as:

$$\Delta H_f(Cr) = E_{tot}(X_2Y_3:Cr) - E_{tot}(host) - \sum_i n_i \mu_i \quad (1),$$

where $E_{tot}(X_2Y_3:Cr)$ (X=Bi, Sb; Y=Se, Te) is the total energy of a supercell with Cr dopants; $E_{tot}(host)$ is the total energy of the supercell without impurities; n_i is the number of certain atoms added

to ($n_i < 0$) or removed from ($n_i > 0$) the supercell; and μ_i is the corresponding chemical potential. In the main text, we take the relative formation energy in reference to the lowest energy among all configurations.

Text B: Influence of supercell size on magnetic coupling constant

Due to the periodic conditions, magnetic interactions not only exist between Cr atoms within the supercell, they also exist among the Cr atoms and their images. In seventh nearest neighbor of 4×4 supercell, the distance (9.984 \AA) between two Cr atoms in the simulation cell and the distance (9.984 \AA) between one Cr atom and the image of the other Cr atom are the same, as shown in Fig. S2. So, the magnetic interaction is indeed long range even. Our further calculations suggest that the existence of the long range magnetic coupling is independent on the simulation cell size. In addition to a (4×4) cell, we tested larger supercell (5×5) to calculate magnetic coupling constant. We found that the magnetic coupling constant is about 7 meV . Inside the 5×5 supercell, the distance between the Cr atoms is still 9.984 \AA . However, the distance between Cr atom and the image in the neighboring cell is about 13.994 \AA (Fig. S2). So, the magnetic coupling still exists, except that it is weakened due to the long distance between the Cr atom and the image atom.

Text C: Spin Orbit Coupling (SOC) effect in slab model

The strong SOC in Bi_2Se_3 and Bi_2Te_3 cause band inversion between valence band and conduction band, and results in different occupations of electrons [4], which may change the long-range magnetic order. Besides, the strong electron-electron correlation for d -electrons of Cr atoms requires introduction of U values to account for the on-site Coulombic interaction. Previously it was found that inclusion of the electron-electron correlation enlarges the band gap and slightly changes the electron occupations [5].

To investigate the effect of SOC and $+U$ on the long-range magnetic order, we performed GGA + U [6] calculations on Cr-doped Bi_2X_3 ($X = \text{Se}, \text{Te}$) with SOC effect included. For one quintuple layer of Bi_2X_3 ($X = \text{Se}, \text{Te}$), a 4×4 unit-cell slab and at least 20 \AA vacuum are included, and $3 \times 3 \times 1$ k -point sampling mesh is adopted. We applied $U = 3 \text{ eV}$ and $J = 0.87 \text{ eV}$ on Cr d -orbitals, which are the same as those used in previous works [5]. The two Cr atoms in the supercell are placed either in the second nearest neighbor (2nd-NN) or in the seventh nearest neighbor (7th-NN). Results are summarized in Fig. S3.

Compared with calculations without SOC effect and $+U$ effect, the ferromagnetic coupling strength in both systems becomes weaker, as $+U$ treatment usually leads to more localized states for d -

orbitals. Nevertheless, the magnetism at the 7th-NN preserves. Although the SOC changes the positions of the p orbitals of Bi and anions, the sp anti-bonding state still mediates the magnetic interactions.

In addition, we calculated the formation energy of Cr-doped Bi_2X_3 ($\text{X}=\text{Se}, \text{Te}$) and included the SOC. The FM configuration at 7th-NN is still the most stable, about 2meV lower than the second lowest energy configuration. However, the most stable configuration of Bi_2Se_3 is still the 2nd-NN, about 3meV lower than the 7th-NN.

Text D: Cr doped bulk Bi_2Te_3

In order to estimate the magnetic order in very thick films, we calculated the formation energy and coupling constants of Cr doped bulk Bi_2Te_3 . As shown in Fig. S4, the first nearest neighbor becomes more stable than seventh neighbor, although the ferromagnetic order of the seventh nearest neighboring configuration preserves. These results are qualitatively consistent with experimental findings that the quantum anomalous Hall effect becomes weaker in $(\text{Bi}_x\text{Sb}_{1-x})_2\text{Te}_3$ thin films with 6 or more quintuple layers [7]. Although substrate and interface may also play important roles in the magnetic order, the simulation cell size is too large in the long range magnetism studies. Therefore, it's impossible for us to directly simulate such effects.

Text E: SOC effect on Cr doped bulk Bi_2Te_3

Effect of SOC on Cr doped bulk Bi_2Te_3 is also calculated and results are shown in Fig. S5. Similar to the case of slab calculations, SOC only changes the relative coupling strength and the relative formation energy. Long range magnetic interactions can still be observed but weaker than the short range ones.

Text F: Partial charge of sp hybridized orbital

The sp hybridization also can be visualized by partial charge density as shown in Fig. S6 (partial charge density of the second band below valence band maximum (VBM)). The sp hybridized orbital around Bi is clearly shown. This hybridized orbital is the step stone state for long range magnetic interaction in Bi_2Te_3 .

Figure S1: (a) The side view of one quintuple layer X_2Y_3 supercell (4×4) with green atoms being Se or Te, yellow and blue atoms being the Bi or Sb in the upper and lower layers respectively. (b) The top view of the upper (yellow) and lower (blue) layer of Bi or Sb.

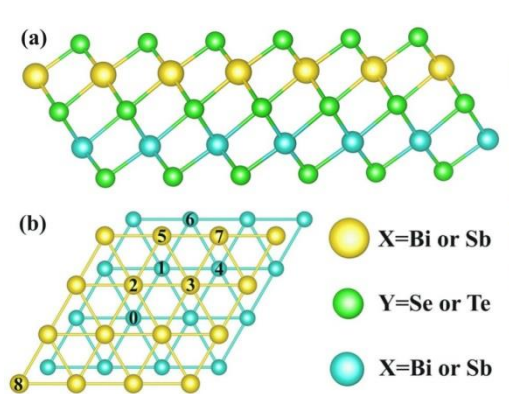


Figure S2: Cr-Cr distance of seventh nearest neighbor (7th-NN) in different supercells. (a) 4×4 supercell (b) 5×5 supercell. Orange atom is Cr, blue atom and yellow atom are Bi in different atomic layer. The dash line is the boundary of the supercell. The Te atoms are removed for clarity. Atom denoted by 1(2) and 3(4) are equivalent atoms in neighboring images. d_{12} is the distance between Cr atoms within the simulation cell and d_{23} is the distance between Cr atom and the image in the neighboring cell.

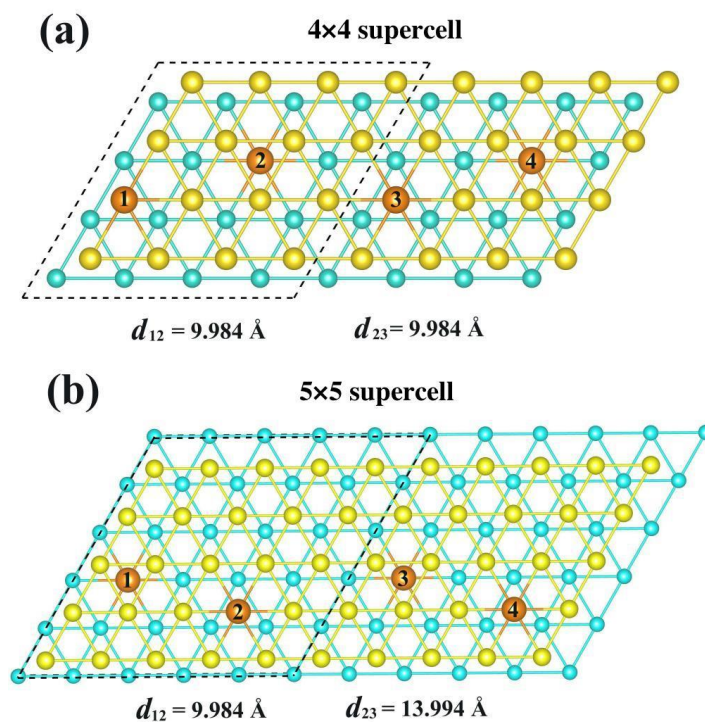


Figure S3: (a) Ferromagnetic coupling constants (defined as half of energy difference between anti-ferromagnetism state and ferromagnetism state) of Cr doped Bi_2Se_3 . (b) Ferromagnetic coupling constants of Cr doped Bi_2Te_3 .

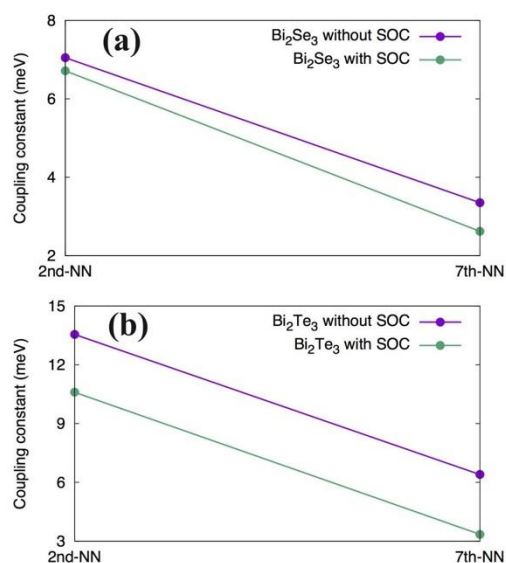


Figure S4: (a) Relative formation energy of Cr doped bulk Bi_2Te_3 . (b) The ferromagnetic coupling constant of the same system.

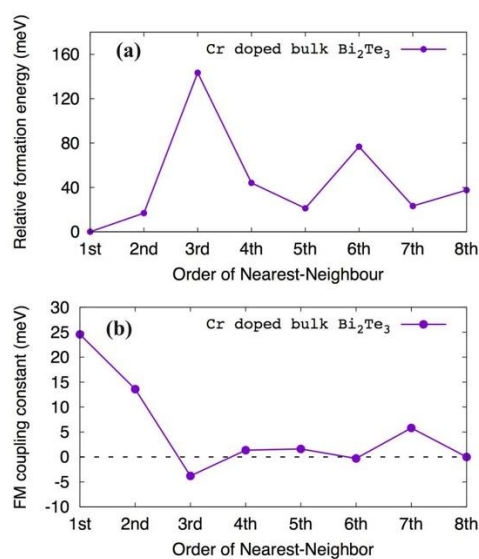


Figure S5: (a) Relative formation energy of Cr doped bulk Bi_2Te_3 with (green line) and without SOC (purple line) included. (b) The ferromagnetic coupling constant of the same system.

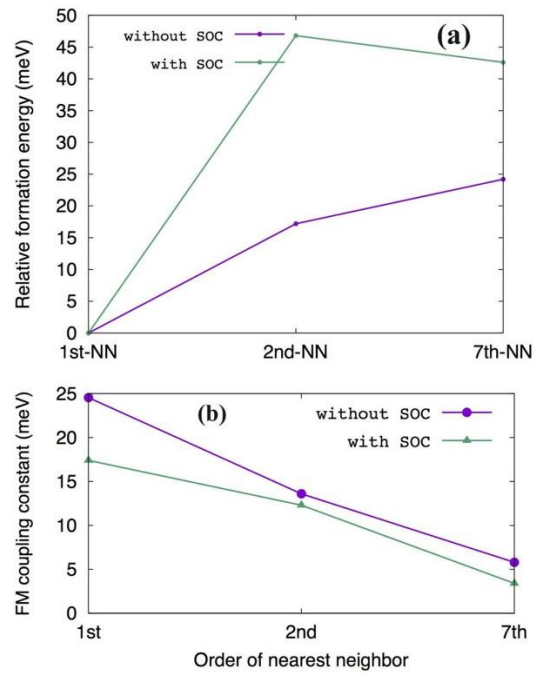
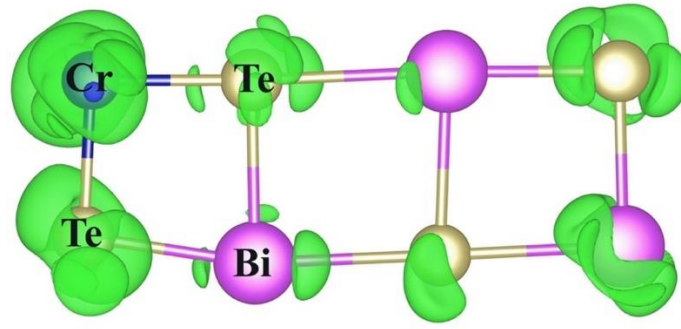


Figure S6: Partial charge density of the second energy band below VBM. Large purple atom is Bi, cinnamon atom is Te, blue atom is Cr. Green part is the partial charge density.



References

- [1] Blöchl P E 1994 *Phys. Rev. B* **50** 17953
- [2] Perdew J P, Burke K, and Ernzerhof M 1996 *Phys. Rev. Lett.* **77** 3865
- [3] Kresse G and Furthmüller J 1996 *Phys. Rev. B* **54** 11169
- [4] Zhang H J *et al.* 2009 *Nat. Phys.* **5** 442
- [5] Zhang J M, Zhu W G, Zhang Y, Xiao D, and Yao Y G 2012 *Phys. Rev. Lett.* **109** 266405

[6] Dudarev S L, Botton G A, Savarsov S Y, Humphreys C J and Sutton A P 1998 *Phys. Rev. B* **57** 1505

[7] Feng X *et al.* 2016 *Adv. Mater.* **28** 6386